Effect of precursor to the physical properties of co-electrodeposited Cu_2ZnSnS_4 thin films

LIYING HAN*, YANG WANG, HONGDONG ZHAO, YATONG ZHOU
Tianjin Key Laboratory of Electronic Materials and Devices, School of Electronics and Information Engineering, Hebei University of Technology, 5340 Xiping Road, Beichen District, Tianjin 300401, P.R. China

The Cu_2ZnSnS_4 (CZTS) thin films is a new type of materials with a band gap of 1.4-1.6 eV, just as the same as the best band gap for solar cells (l.5eV). The co-electrodeposition is a one-step method for the preparation of Cu_2ZnSnS_4 thin films on ITO substrate. Through the simple and effective co-electrodeposition method, the structural, morphological, compositional and optical properties of Cu_2ZnSnS_4 thin films can be regulated through adjusting the Cu, Zn, Sn and S component in the precursor solution. Structure and morphological characteristics of the Cu_2ZnSnS_4 thin films were studied by XRD diffraction analysis, Raman analysis, EDS and SEM analysis respectively. The photoelectric response analysis also were performed to comprehensive evaluate the quality of the thin films.

(Received March 18, 2017; accepted November 28, 2017)

Keywords: CZTS, Thin film, Co-electrodeposition, Precursor

1. Introduction

Quaternary compound semiconductor Cu_2ZnSnS_4 (CZTS) is a kind of eco-friendly solar cell materials with non-toxic elements. It has a band gap energy of 1.4-1.6 eV and optical absorption coefficient over 10^4 cm^{-1}[1,2]. The structure of CZTS is similar to that of CIGS and the photoelectric conversion efficiency of CZTS solar cell is theoretically concluded more than 32%, according to Shockley-Queisser photon balance calculations [3]. Obviously, the CZTS thin films are promising when used in the field of photovoltaic battery materials. Therefore, there are lots of experimental techniques for the preparation of CZTS thin films: sputtering [4], thermal evaporation [5], photo-chemical deposition [6], spray deposition technique [7], spray pyrolysis technique [8], sulfurization of electron-beam-evaporated precursors [9]. However, the costs of these experimental techniques are very high mostly. They will consume large amounts of energy and the raw materials. In addition, some techniques are harmful to the environment and human body. Electrochemical deposition for the preparation of CZTS thin film should be the most appropriate choice which has the following advantages: deposition can be performed on complex substrate; working temperature is room temperature or a little higher than room temperature; the quantity of depositional thin films could be controlled by electrochemical deposition cycle, so the thickness and composition of thin films can be controlled conveniently. Therefore, the co-electrodeposition for the preparation of CZTS thin films is a simple and effective method, which omits the intermediate preparation process of nanoparticles and is performed at room temperature. The thin films followed by sulfur diffusion resulted in a optical band gap of 1.5eV, which demonstrated the potential in the application as the absorber of photovoltaic device.

Electrochemically deposited CZTS thin films for solar cells has drawn more attention recently. A solar cell had 3.2-3.4% power conversion efficiency for electrochemically deposited CZTS solar cells was reported in 2012 [11]. A 11.1% efficiency for CZTS based solar cells was reported [12]. IBM also reported 7.3% efficiencies for CZTS solar cells prepared from electrochemically deposited [13]. However, the effects of metal and sulfur precursors to the physical properties of electrodeposited CZTS thin films were still not well studied.

In this paper, co-electrodeposition of all constituents Cu, Zn, Sn, S was performed. The as-deposited thin films would be adjusted by changing the dosage of copper, zinc, tin, and sulfur precursor. Currently, there were little reports on the effects of precursors to the physical properties of CZTS thin films. It is significant to find the optimal dosage of precursor for preparing CZTS thin films with rich-Zn and poor-Cu [14-16].

2. Experimental details

2.1. Materials

Copper sulfate pentahydrate, zinc sulfate heptahydrate, stannous chloride hydrate, sodium thiosulfate pentahydrate, trisodium citrate dihydrate and disodium tartrate dihydrate are all of analytical grade and purchased from Sinopharm chemical LTD (Shanghai).

2.2. Deposition of CZTS thin films

In a typical co-electrodeposition, the electrochemical cell was used which consists of a CHI1140A electrochemical workstation (CH Instrument, USA) and a

conventional three-electrode assembly with a platinum foil counter electrode, an Ag/AgCl reference electrode and ITO glass substrates working electrode. The CZTS thin films for this study were deposited onto ITO glass substrates (2×2 cm^2). Before deposition, the ITO glass substrates were cleaned ultrasonically in acetone, ethanol and distilled water and finally dried by flowing nitrogen. The precursor solution was stirred well to form clear liquid which contains $CuSO_4 \cdot 5H_2O$, $ZnSO_4 \cdot 7H_2O$, $SnCl_2 \cdot 2H_2O$, $Na_2S_2O_3 \cdot 5H_2O$, $C_4H_4Na_2O_6$ (0.01M) and $Na_3C_6H_5O_7$ (0.2M). The dosage of copper, zinc, tin and sulfur precursor are referred from table 1. Sodium citrate and sodium amount tartrate are used as acidity regulator. The deposition of the CZTS thin films was performed at -1.05V versus Ag/AgCl for 15 min. The deposition potential of CZTS thin film was estimated from cyclic voltammetry of the precursor solution. According to table 1, adjusting the usage amount of metal and sulfur precursor in the precursor solution resulted in different thin films [17]. After deposition, the as-deposited films were washed by deionized water and dried under flowing nitrogen. At 500 °C, the annealing treatment was performed for the as-deposited films in the atmosphere of N_2/H_2S (5%) for 30mins. Then the as-deposited films were cooled down naturally to room temperature in the annealing furnace.

Table1. The composition content of each precursor in aqueous solution.

Component (mM)	$CuSO_4 \cdot 5H_2O$	$ZnSO_4 \cdot 7H_2O$	$SnCl_2 \cdot 2H_2O$	$Na_2S_2O_3 \cdot 5H_2O$
CZTS-Cu1	6	15.75	7.5	11.25
CZTS-Cu2	6.75	15.75	7.5	11.25
CZTS-Cu3	7.5	15.75	7.5	11.25
CZTS-Cu4	8.25	15.75	7.5	11.25
CZTS-Zn1	7.5	14.625	7.5	11.25
CZTS-Zn2	7.5	15.1875	7.5	11.25
CZTS-Zn3	7.5	15.75	7.5	11.25
CZTS-Zn4	7.5	16.3125	7.5	11.25
CZTS-Sn1	7.5	15.75	6	11.25
CZTS-Sn2	7.5	15.75	6.75	11.25
CZTS-Sn3	7.5	15.75	7.5	11.25
CZTS-Sn4	7.5	15.75	8.25	11.25
CZTS-S1	7.5	15.75	7.5	10.5
CZTS-S2	7.5	15.75	7.5	10.875
CZTS-S3	7.5	15.75	7.5	11.25
CZTS-S4	7.5	15.75	7.5	11.625

2.3. Fabrication of CZTS solar cells

CZTS thin-film photovoltaic devices were fabricated with a conventional sandwich-type glass/Mo/Cu_2ZnSnS_4/CdS/ZnO/Al-doped ZnO (AZO) configuration. A Mo-coated glass substrate was prepared by DC magnetron sputtering with a film thickness of 500 nm. A thick layer of kesterite Cu_2ZnSnS_4 nanocrystals was evenly deposited onto the Mo-coated glass substrate by above co-electrodeposition method. Then the film was sintered at 500 °C in N_2 atmosphere for 30 mins in a quartz tube. A CdS buffer layer with a thickness of about 80 nm was formed by chemical bath deposition using a solution containing 34 mL of deionized water, 5.5 mL of 0.004 M $CdSO_4$ solution, 5.5 mL of 1.89 M thiourea solution, and 7 mL of stock NH_4OH solution. Next a thin 50 nm intrinsic ZnO film capped with a 150 nm high-conductivity AZO layer was deposited by magnetron sputtering. An Al grid (500 nm) was deposited as a current collector by electron beam evaporation onto the AZO layer, with the remaining surface acting as an active area of 0.5 cm^2.

2.4 Characterization of CZTS thin films and solar cells

The structural properties of the as-deposited films were identified by X-ray diffractometer (XRD, Rigaku D/max 220 kV, Cu Ka: k = 0.154 nm) and Raman spectra (514.5 nm, JY, H800UV) were measured to analyze the phase purities of the as-deposited films. The morphologies of CZTS thin films were characterized by scanning electronic microscope (SEM, FEI Sirion 200). The EDS data were measured with SEM (Hitachi Su-1500). For every sample, the EDS data were measured four times and the averaged results were used as the final data. The absorption spectra was measured with UV-Vis spectrophotometer (Jasco UV-570). The current density-voltage (J-V) characteristics of the CZTS-based solar cell were measured using a solar simulator under air mass (AM) 1.5 and 100 mW/cm2 illumination.

3. Results and discussions

3.1. Structural and morphological analysis of CZTS thin film

Fig. 1 shows component dependent EDS of as-deposited CZTS-Cu1, CZTS-Cu2, CZTS-Cu3 and CZTS-Cu4 thin films and component dependent EDS, XRD and Raman spectra of annealed CZTS-Cu1, CZTS-Cu2, CZTS-Cu3 and CZTS-Cu4 thin films. From Fig. 1 (a), with the increasing of the usage amount of Cu precursor, the atomic ratio of Zn, Sn and S in as-deposited CZTS thin films has a very little fluctuation near 20 % and the ratio increasingly approaches equal. Differently, the atomic ratio of Cu shows an obvious increasing trend. After the annealing treatment was performed for the as-deposited films in the atmosphere of N_2/H_2S (5%) at 500 °C for 30 mins, the ratio of Cu/Zn/Sn/S is basically matched to 2:1:1:4 of the CZTS stoichiometric ratio and the atomic ratio of Cu has a very little increasing trend with the increasing of the usage amount of Cu precursor, as shown in Fig. 1(b). From the XRD pattern (Fig. 1 (c)) of the annealed CZTS-Cu1, CZTS-Cu2, CZTS-Cu3 and CZTS-Cu4 thin film, peaks at 28.45°, 32.78°, 47.35° and 56.24° correspond to (112), (200), (220) and (312) planes of kesterite structured CZTS (PDF#26-0575) [18]. These peaks at 26.49°, 33.59°, 37.73° and 51.49° are arisen from ITO substrates [19]. In addition, impurity peaks from

$Cu_{2-x}S$ phases are observed at 29.33° (PDF#06-0464), 31.81° (PDF#06-0464), 46.18° (PDF#36-0380), 52.69° (PDF#06-0464) and 54.53° (PDF#47-1748) [20]. From CZTS-Cu1 to CZTS-Cu4, impurity peaks from $Cu_{2-x}S$ phases becomes strong in turn. Especially, these impurity peaks are relatively obvious in the XRD pattern of CZTS-Cu4 thin film and unconspicuous in the XRD pattern of CZTS-Cu1 thin film. Above results shows that impurity $Cu_{2-x}S$ phases appeared when there is too much Cu precursor in solution which resulted in the Cu-rich thin films. In Fig. 1 (d), Raman peaks at 286.1 cm^{-1}, 336.2 cm^{-1} and 371.1 cm^{-1} are belonged to the 'kesterite' structural CZTS [21,22]. While raman peaks at 474.4 cm^{-1} and 495.7 cm^{-1} are belonged to impurity $Cu_{2-x}S$ phases [23,24]. The Raman spectra of the annealed CZTS-Cu1, CZTS-Cu2, CZTS-Cu3 and CZTS-Cu4 thin film verifies the conclusion of XRD diffraction analysis. Therefore, the usage amount (6mM) of Cu precursor for CZTS-Cu1 should be selected for the preparation of Cu-poor thin films.

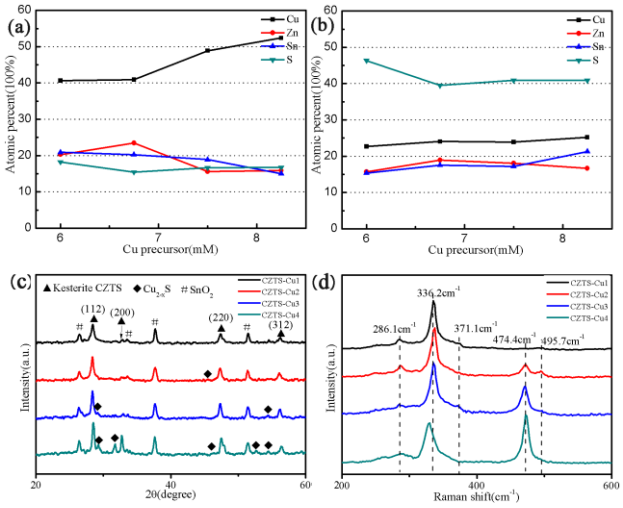

Fig. 1. (a) Component dependent EDS of the unannealed CZTS-Cu1, CZTS-Cu2, CZTS-Cu3 and CZTS-Cu4 thin film and (b) Component dependent EDS, (c) XRD and (d) Raman spectra of the annealed CZTS-Cu1, CZTS-Cu2, CZTS-Cu3 and CZTS-Cu4 thin film

Fig. 2 shows the SEM morphology of the as-deposited and annealed CZTS-Cu1, CZTS-Cu2, CZTS-Cu3 and CZTS-Cu4 thin films. In these SEM images of Fig. 2(a_1-d_1), the particle sizes of unannealed CZTS films are between 0.5mm to 2mm. All particle present irregular spherical particles and many voids are observed which shows that the thin film is not pyknotic. With the increase of Cu^{2+} concentrations in solutions, more and more big conglobatus particles appear in the films, especially in Fig. 2(d_1). When the annealing treatment was performed, the H_2S participated in reaction which made the dispersed particle combine and grow up. As showed in Fig. 2(a_2-d_2), the number of spherical particles decrease and their outline become blurred. Obviously, the annealed films have higher densities and larger particle size.

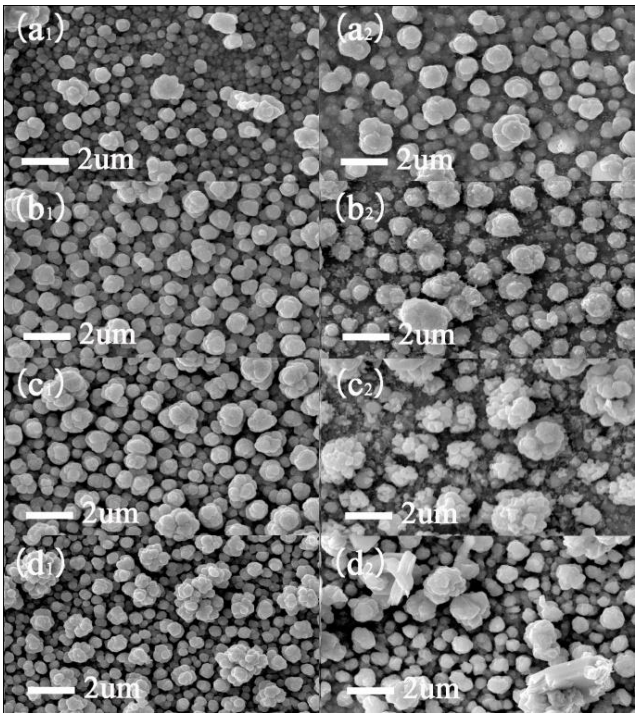

Fig. 2. SEM morphology of the (a1-d1) unannealed and (a2-d2) annealed CZTS-Cu1, CZTS-Cu2, CZTS-Cu3 and CZTS-Cu4 thin film.

Fig. 3 shows component dependent EDS of as-deposited CZTS thin film and component dependent EDS, XRD and Raman spectra of annealed CZTS thin film. With the increase of Zn^{2+} concentrations in solutions, Fig. 3 (a) shows that the atomic ratio of Zn in as-deposited CZTS thin films have not obvious change and the ratio of Cu/Zn/Sn/S of annealed CZTS is near to 2:1:1:4. The XRD (Fig. 3 (c)) and Raman spectra (Fig. 3 (d)) also suggest the existence of impurity $Cu_{2-x}S$ phases besides the 'kesterite' structural CZTS in the annealed thin films. With the increasing of the usage amount of Zn precursor, the change rule for the ratio of Zn (Fig. 3 (b)) in the annealed thin films is similar to that of Cu (Fig. 1 (b)) which is increased slightly. There are no obvious XRD and raman peaks which belong to impurity ZnS phases found in (Fig. 3 (b, d)), but peaks of impurity $Cu_{2-x}S$ phases decreased in turn from CZTS-Zn1 to CZTS-Zn4. And Fig. 3 (b) shows that the ratio of Zn in the annealed CZTS-Zn4 thin films reach to 19%. So the usage amount (16.3125 mM) of Zn precursor for CZTS-Zn4 should be selected for the preparation of Zn-rich thin films.

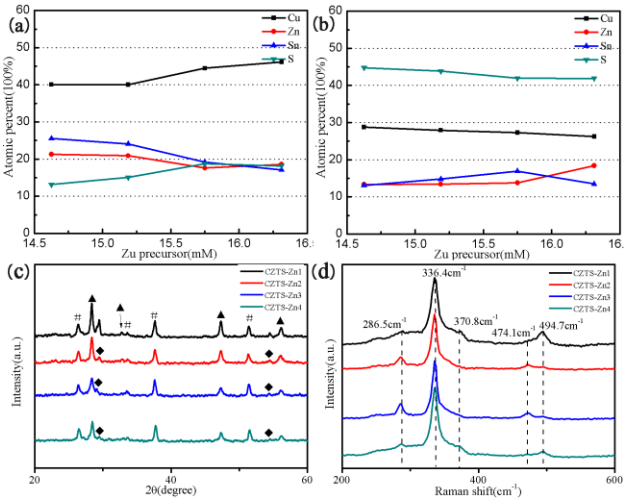

Fig. 3. (a) Component dependent EDS of the unannealed CZTS-Zn1, CZTS-Zn2, CZTS-Zn3 and CZTS-Zn4 thin film and (b) Component dependent EDS, (c) XRD and (d) Raman spectra of the annealed CZTS-Zn1, CZTS-Zn2, CZTS-Zn3 and CZTS-Zn4 thin film.

Fig. 4 shows the SEM morphology of the as-deposited and annealed CZTS- Zn1, CZTS-Zn2, CZTS-Zn3 and CZTS- Zn4 thin film. The annealed thin films (Fig. 4(a_2-d_2)) shows higher density than that of unannealed thin films (Fig. 4(a_1-d_1)). This also resulted from the participation in reaction of H_2S which made particle combine and particle boundary reduced. With the increasing of the usage amount of Zn precursor, it is easy to find that the quality of the annealed thin films is better and better which has higher density and less clearance. As shown in Fig. 4(a_1, a_2), too large particles and more gap maybe resulted from too much using of Cu precursor . While the annealed CZTS- Zn4 thin film owns the highest quality in Fig. 4(d_2).

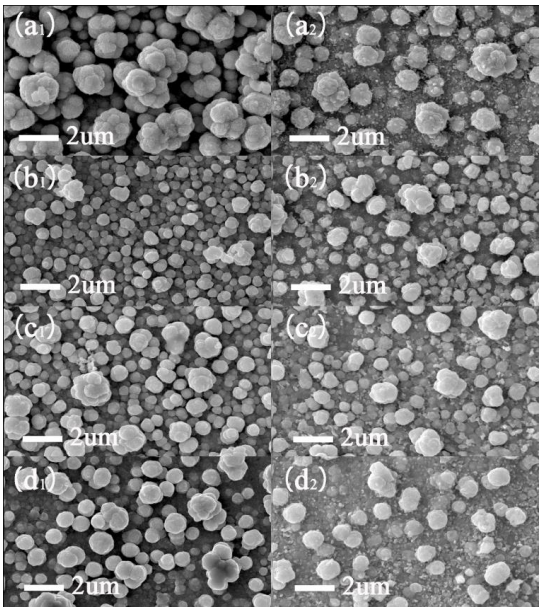

Fig. 4. SEM morphology of the (a1-d1) unannealed and (a2-d2) annealed CZTS-Zn1, CZTS-Zn2, CZTS-Zn3 and CZTS-Zn4 thin film.

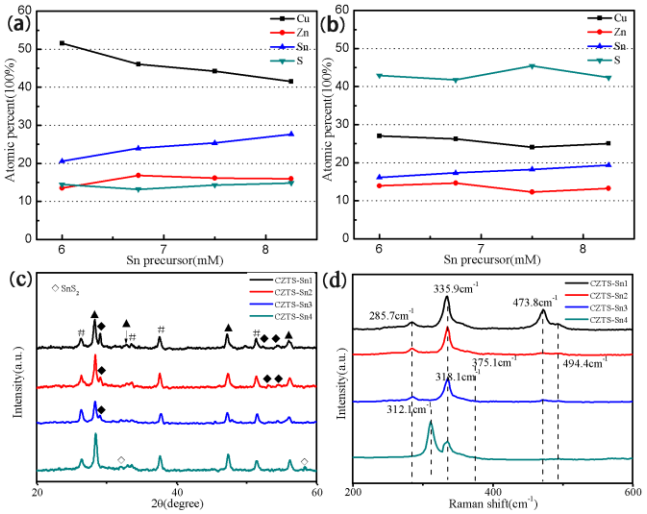

Fig. 5. (a) Component dependent EDS of the unannealed CZTS-Sn1, CZTS-Sn2, CZTS-Sn3 and CZTS-Sn4 thin film and (b) Component dependent EDS, (c) XRD and (d) Raman spectra of the annealed CZTS-Sn1, CZTS-Sn2, CZTS-Sn3 and CZTS-Sn4 thin film

Fig. 5 shows (a) component dependent EDS of the unannealed CZTS-Sn1, CZTS-Sn2, CZTS-Sn3 and CZTS-Sn4 thin film and (b) component dependent EDS, (c) XRD and (d) Raman spectra of the annealed CZTS-Sn1, CZTS-Sn2, CZTS-Sn3 and CZTS-Sn4 thin film. Fig. 5(a, b) show that no matter the thin film was annealed or unannealed, the atom ratio of Sn increases with the increasing of the usage amount of Sn precursor. After the annealed process, the atomic ratio of S increases and the atomic ratio of Cu decreases in a large scale which makes the ratio of Cu/Zn/Sn/S tend to stoichiometric ratio. Fig. 5(c, d) show that the impurity phase still is $Cu_{2-x}S$ and the impurity peaks gradually weaken with the increasing of the usage amount of Sn precursor. In Fig. 5(d), the Raman spectra of the annealed CZTS-Sn4 thin film suggests the existence of impurity SnS_2 phase at 312.1cm^{-1}. In Fig. 5(c), peaks which are at 32.13°and 58.37° corresponding to the (102) and (200) planes of SnS_2 (PDF#21-1231) also could be observed. In all, the usage amount (7.5mM) of Sn precursor for CZTS-Sn3 should be selected for the preparation of thin films with high quality.

From the SEM morphology of the (a_1-d_1) unannealed and (a_2-d_2) annealed CZTS-Sn1, CZTS-Sn2, CZTS-Sn3 and CZTS-Sn4 thin film in Fig 6, it can be seen that particle size and morphology have not much difference. After an annealing process, the thin films also became denser. But there is a interesting phenomenon that the morphology of CZTS-Sn3 and CZTS-Sn4 thin film change from irregular sphere to sheet shapes, especially for CZTS-Sn4 thin film. In Fig. 6(d_2) Some large particles like flower assembled by flake and irregular particles may be impurity SnS_2 phase, which verifies the results of the XRD and Raman measurements.

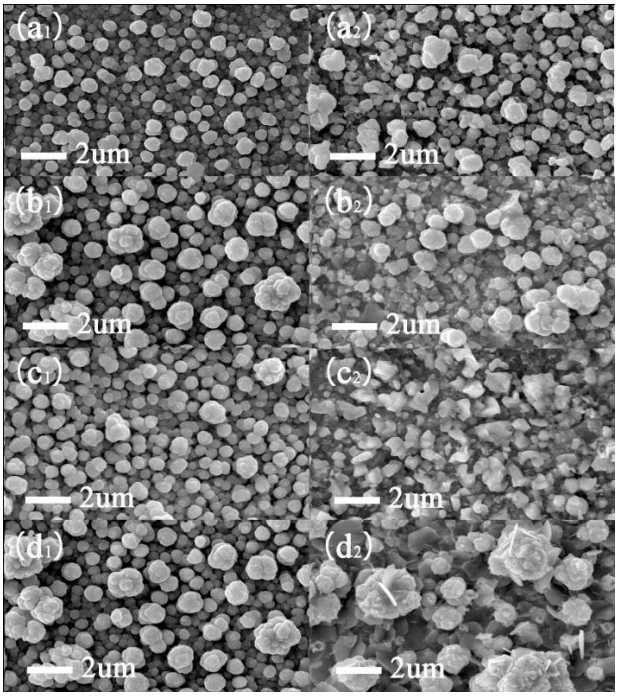

Fig. 6. SEM morphology of the (a1-d1) nonannealed and (a2-d2) annealed CZTS-Sn1, CZTS-Sn2, CZTS-Sn3 and CZTS-Sn4 thin film

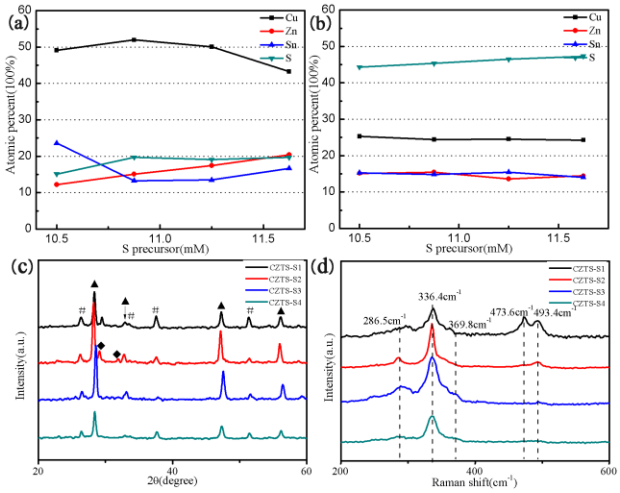

Fig. 7. (a) Component dependent EDS of the nonannealed CZTS-S1, CZTS-S2, CZTS-S3 and CZTS-S4 thin film and (b) Component dependent EDS, (c) XRD and (d) Raman spectra of the annealed CZTS-S1, CZTS-S2, CZTS-S3 and CZTS-S4 thin film

Fig. 7 shows (a) component dependent EDS of the unannealed CZTS-S1, CZTS-S2, CZTS-S3 and CZTS-S4 thin film and (b) component dependent EDS, (c) XRD and (d) Raman spectra of the annealed CZTS-S1, CZTS-S2, CZTS-S3 and CZTS-S4 thin film. Fig. 7 (a, b) show that the ratio of Cu/Zn/Sn/S accord with stoichiometric ratio after annealing. The XRD patterns of the annealed CZTS-S3 and CZTS-S4 thin film have not obvious peaks of impurity $Cu_{2-x}S$ phases and the Raman spectra of the annealed CZTS-S4 thin film has only one obvious peak at 336.4cm^{-1} which belongs to the 'kesterite' structural CZTS. So the XRD (Fig. 7 (c)) and Raman spectra (Fig. 7 (d)) of the annealed thin film suggest that impurity $Cu_{2-x}S$ phases gradually disappeared with the increasing of the usage amount of S precursor after annealing. So the usage amount (11.625mM) of S precursor for CZTS-S4 is the most suitable for the preparation of thin films without impurity $Cu_{2-x}S$ phases. After an annealed process, the thin films also have higher density and less clearance. The morphology of particle changes with bigger size, as shown in Fig. 8.

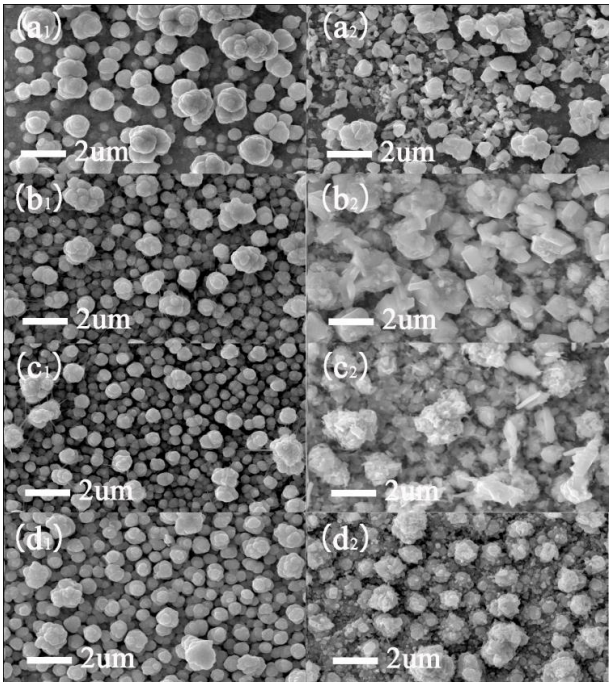

Fig. 8. SEM morphology of the (a1-d1) nonannealed and (a2-d2) annealed CZTS-S1, CZTS-S2, CZTS-S3 and CZTS-S4 thin film.

3.2. Optical studies and photo-electrochemical measurement of CZTS thin film

The UV-Vis absorption spectra of the as-deposited thin films were investigated and the UV-Vis absorption spectra of a CZTS-S4 is shown in Figure 9. Fig. 9 indicates that the UV-Vis absorption spectra of the annealed CZTS thin films exhibit a broad absorption in the visible region and a tail extending to longer wavelengths. The band gap values of all the samples were determined to be 1.48-1.54 eV by plotting $(Ah\nu)^2$ versus $h\nu$ (A = absorbance, h = Planck's constant and ν = frequency) and extrapolating the linear portion of the spectrum in the band edge region [25], as shown in the inset of Fig. 9. These values match well with the reported 1.4-1.6 eV values for 'kesterite' structural CZTS [26]. Figure 10 shows the J-V characteristic of the best performance CZTS-based solar cell which active area was 0.3 cm^2 presenting η =1.23% with open-circuit voltage (V_{oc}) = 510 mV, short-circuit current density (J_{sc})= 4.98 mA/cm^2, filling factor (FF) =48.4% .

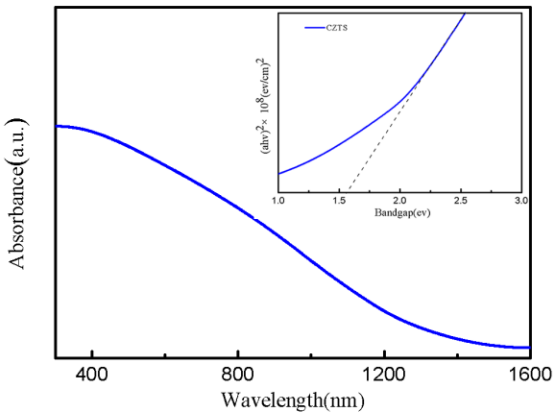

Fig. 9. UV-Vis absorption spectrum of CZTS thin film. The inset image shows a band gap of 1.54 eV

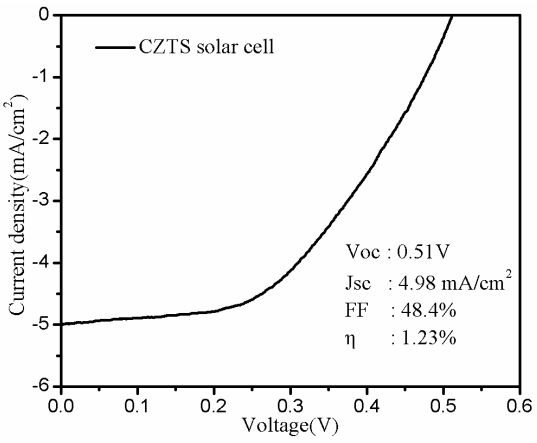

Fig. 10. J-V characteristics of the best performance CZTS thin film solar cell.

4. Conclusions

In summary, CZTS thin films with 'kesterite' structure were prepared by a simple co-electrodeposition method. With the increasing of the usage amount of Cu, Zn, Sn and S precursor, EDS measurements show that the atom ratio of Cu, Zn, Sn and S of the annealed CZTS thin films have a rising trend, respectively. The ratio of Cu/Zn/Sn/S is near to 2:1:1:4 of the CZTS stoichiometric ratio. XRD and Raman measurements confirmed the kesterite structure and the existence of impurity $Cu_{2-x}S$ phases in annealed CZTS thin films. The UV-Vis absorption spectra suggested the as-deposited thin films have a broad absorption in the visible region with band gap values of 1.48-1.54 eV. The best performance CZTS-based solar cell shows a power conversion efficiency of 1.23%.

Acknowledgements

We acknowledge Tianjin Key Laboratory of Electronic Materials and Devices of Hebei University of Technology for the help of characterization works.

References

[1] C. L. Azanza Ricardo, M. S. Su'ait, M. Müller, P. Scardi, J. Power Sources. **230**, 70 (2013).
[2] L. J. Chen, Y. J. Chuang, J. Power Sources **241**, 259 (2013).
[3] T. K. Todorov, J. Tang, S. Bag, O. Gunawan, T. Gokmen, Y. Zhu, D. B. Mitzi, Adv. Energy Mater. **3**, 34 (2013).
[4] T. P. Dhakal, C. Y. Peng, R. R. Tobias, et al., Solar Energy **100**, 23 (2014).
[5] C. Shi, G. Shi, Z. Chen, et al. Mater. Lett. **73**, 89 (2012).
[6] K. Moriya, K. Tanaka, H. Uchiki, Jpn. J. Appl. Phys. **44**(1S), 715 (2005).
[7] Y. B. K. Kumar, G. S. Babu, P. U. Bhaskar, et al. Sol. Energy Mater. Sol. Cells. **93**(8), 1230 (2009).
[8] S. M. Bhosale, M. P. Suryawanshi, M. A. Gaikwad, et al., Mater. Lett. **129**, 153 (2014).
[9] T. Tanaka, T. Nagatomo, D. Kawasaki, et al. J. Phys. Chem. Solids. **66**(11), 1978(2005).
[10] S. M. Pawar, B. S. Pawar, A. V. Moholkar, et al., Electrochim. Acta **55**(12), 4057 (2010).
[11] A. Ennaoui, M. Lux-Steiner, A. Weber, et al. Thin Solid Films **517**(7), 2511 (2009).
[12] Teodor K. Todorov, Jiang Tang, Santanu Bag, Oki Gunawan, Tayfun Gokmen,Yu Zhu, David B. Mitzi. Adv. Energy Mater. **3**, 34(2013).
[13] L. Guo, Y. Zhu, O. Gunawan, et al. Prog. Photovolt. Res. Appl. **22**(1), 58 (2014).
[14] S. Chen, X. G. Gong, A. Walsh, S. H. Wei, Appl. Phys. Lett. **94**, 041903 (2009).
[15] S. M. Pawar, B. S. Pawar, A. V. Moholkar, D. S. Choi, J. H. Yun, J. H. Moon, S. S. Kolekar, J. H. Kim, Electrochim. Acta. **55**, 4057 (2010).
[16] A. Ennaoui, M. Lux-Steiner, A. Weber, D. Abou-Ras, I. Kotschau, H. W. Schock, R. Schurr, A. Holzing, S. Jost, R. Hock, T. Voss, J. Schulze, A. Kirbs, Thin Solid Films **517**, 2511 (2009).
[17] X. C. He, H. L. Shen, W. Wang, B. S. Zhang, Y. M. Dai, Y. B. Lu, J. Mater. Sci: Mater. Electron. **24**, 572 (2013).
[18] S. N. Park, S. J. Sung, D. H. Son, et al., RSC Advances **4**(18), 9118 (2014).
[19] Y. Wang, J. Ma, P. Liu, et al. Mater. Lett. **77**, 13 (2012).
[20] P. A. Fernandes, P. M. P. Salomé, A. F. Da Cunha, Semicond. Sci. Technol. **24**(10), 105013 (2009).

[21] X. He, H. Shen, J. Pi, et al., Sci.-Mater. Electron. **24**(11), 4578 (2013).
[22] A. Wangperawong, J. S. King, S. M. Herron, et al., Thin Solid Films **519**(8), 2488 (2011).
[23] P. A. Fernandes, P. M. P. Salomé, A. F. Da Cunha, Thin Solid Films **517**(7), 2519 (2009).
[24] H. Yoo, J. H. Kim, L. Zhang, Curr. Appl. Phys. **12**(4), 1052(2012).
[25] Q. W. Tian, Y. Cui, G. Wang, D. C. Pan, RSC Adv. **5**, 4184 (2015).
[26] M. Cao, Y. Shen, J. Cryst. Growth. **318**(1), 1117 (2011).

*Corresponding author: lizhi_han@hebut.edu.cn